Hydrogen-iodide decomposition over Pd-CeO_2 nanocatalyst for hydrogen production in sulfur-iodine thermochemical cycle

Amit Singhania[a], Venkatesan V. Krishnan[b], Ashok N. Bhaskarwar[a*], Bharat Bhargava[c], Damaraju Parvatalu[c]

[a]*Department of Chemical Engineering, Indian Institute of Technology, Delhi, Hauz Khas, New Delhi 110016, INDIA*

[b]*School of Science and Engineering, Teesside University, Middlesbrough, TS1 3BA, UK*

[c]*ONGC Energy Centre, 2nd Floor, Core-2, Scope Minar, New Delhi 110092, INDIA*

Abstract

A highly active and stable catalyst for hydrogen-iodide decomposition reaction in sulfur-iodine (SI) cycle has been prepared in the form of Pd-CeO_2 nanocatalyst by sol-gel method with different calcination temperatures (300°C, 500°C, and 700°C). XRD and TEM confirmed a size around 6-8 nm for Pd-CeO_2 particles calcined at 300°C. Raman study revealed large number oxygen vacancies in Pd-CeO_2-300 when compared to Pd-CeO_2-500 and Pd-CeO_2-700. With increase in calcination temperature, the average particle size increased whereas the specific surface area and number of oxygen vacancies decreased. Hydrogen-iodide catalytic-decomposition was carried out in the temperature range of 400°C-550°C in a quartz-tube, vertical, fixed-bed reactor with 55 wt % aqueous hydrogen-iodide feed over Pd-CeO_2 catalyst using nitrogen as a carrier gas. Pd-CeO_2-300 showed hydrogen-iodide conversion of 23.3 %, which is close to the theoretical equilibrium conversion of 24 %, at 550°C. It also showed a reasonable stability with a time-on-stream of 5 h.

Keywords: Hydrogen-iodide decomposition; Palladium; Ceria; Catalytic activity; Hydrogen production; Sulfur-iodine cycle

[*]Corresponding author. Tel.: +91-011-26591028

E-mail address: ashoknbhaskarwar@yahoo.co.in

1. Introduction

Sulfur-iodine (SI) cycle is considered as a promising technology for the production of large quantities of hydrogen by thermochemical water splitting. Hydrogen is a viable alternative to fossil fuels, since it is a cheap, renewable, and clean source of energy. Researchers have fully realized the utility of SI cycle [1-3]. The SI cycle consists of the following three reactions:

$SO_2(g) + I_2(s) + 2H_2O(l) \leftrightarrow 2HI(aq) + H_2SO_4(aq)$ (T= 20°C-120°C; ΔH= -75±15 kJ mol^{-1})…(1)

$H_2SO_4(g) \leftrightarrow H_2O(g) + SO_2(g) + ½\ O_2(g)$ (T= 800°C-900°C; ΔH= 186±3 kJ mol^{-1})…(2)

$2HI(g) \leftrightarrow H_2(g) + I_2(g)$ (T= 300°C-500°C; ΔH~12 kJ mol^{-1})…(3)

The overall reaction is the splitting of water into hydrogen and oxygen, without emission of any greenhouse gases, and hence it is a potentially sustainable means to a clean fuel. The iodine and sulphur dioxide produced in hydrogen-iodide decomposition reaction (3) and sulphuric-acid decomposition reaction (2), respectively, are recycled back to Bunsen reaction (1). Thermodynamically, hydrogen-iodide decomposition is a limiting reaction step, being a reversible reaction. A considerable amount of energy is required in this step along with a highly active and stable catalyst for the production of hydrogen in the highly corrosive hydrogen-iodide environment.

Different types of monometallic catalysts (precious Pt, Au, Pd, Ru, and Ir metals and non-precious Ni, Mo, and Co metals) [4-7], and bimetallic catalysts (Ni-Pt, Ni-Pd, Pt-Ir, Pd-Ir, and Pt-Ru) [8-11] have been reported in the literature for hydrogen-iodide decomposition reaction. Various support materials such as ceria, zirconia, γ-alumina, activated carbon (AC), carbon nanotubes (CNTs), carbon molecular sieves (CMS), and graphite [12-16] have also been reported. O'Keeffe et al. [6] presented an overview of different catalysts used for hydrogen-iodide decomposition reaction and revealed that Pt supported catalysts possessed a high activity. Precious metal based catalysts (supported Pt, Pd, and Ir catalysts) have also been studied extensively for this reaction [11, 17, 18]. Few reports have shown that the activity of Pt supported catalyst was influenced by the support [19]. Some results showed that Pt catalyst showed agglomeration, and was not stable in the corrosive

hydrogen-iodide environment [19-21].

Ceria has frequently been used for hydrogen-iodide decomposition as it is non-toxic, cheap, abundant, and has some interesting physicochemical properties. Ceria is attractive as catalyst or as support (especially at nanoscale) due to the presence of a large number of lattice defects (oxygen vacancies, dislocations, and grain and interphase boundaries) [22]. It has been used in various applications such as gas sensor, automotive catalyst, solid electrolyte, and catalyst/ support [23-25]. It is used mainly because of its oxygen storage capacity and its interaction with precious metals [26, 27]. Lot of research has focused on interaction between precious metals and pure ceria [22]. Zhang et al. [26] and Fan et al. [27] reported the insertion of precious metal ions into ceria lattice with the help of sol-gel method which brings a different synergistic effect (high oxygen mobility in support, and larger reducibility of precious metals). Thus, insertion of precious metals might result in an increase in oxygen vacancies and oxygen mobility and improve the catalytic activity.

In this paper, palladium is chosen an active catalytic ingredient with ceria because it is much cheaper than Pt (Pt: 975 USD per oz, and Pd: 799 USD per oz) [28]. Ni is also a cheaper option to Pd, and has been explored by us earlier, but stability is an issue with Ni for hydrogen-iodide decomposition reaction [6]. Pd-CeO_2 can be prepared by different synthesis methods such as sol-gel [29], reverse micellar [30], sonochemical [31], hydrothermal [32], combustion [33], and precipitation routes [26]. As far as the authors are aware, this is the first time that the combination of Pd and CeO_2 nanocatalysts has been used for hydrogen-iodide decomposition reaction in the thermochemical SI cycle. The idea is to investigate the performance of Pd-CeO_2 catalysts, synthesized by sol-gel method with different calcination temperatures, for hydrogen-iodide decomposition. Furthermore, the characterization data of Pd-CeO_2 catalysts by BET, XRD, TEM, ICP-AES, and RAMAN spectroscopy have been reported here.

2. Experimental Work

2.1. Catalyst preparation

For the preparation of Pd-CeO_2 catalysts by the sol-gel technique, citric acid and cerium nitrate hexahydrate were maintained in a ratio of 1.5. Required amount of ethylene glycol (15 wt % of citric acid); 0.5 g was taken in a beaker containing mixture of cerium nitrate hexahydrate, palladium chloride (mass ratio of Ce:Pd = 98:2), and citric acid, and stirred at 60°C until spongy yellow gel formed. The spongy-gel was then dried at 90°C for 12 h. The product was then calcined at different temperatures, namely, 300°C, 500°C, and 700°C, each for 4 h. The Pd-CeO_2 catalysts prepared by this method are denoted by Pd-CeO_2–300, Pd-CeO_2–500, and Pd-CeO_2–700, respectively. The measurement by ICP-AES confirmed that the mass percentage of Pd in the catalyst was 2%.

2.2. Catalyst characterization

BET instrument was used to measure the specific surface areas of the prepared catalysts (Micrometrics, ASAP 2010). XRD data of Pd-CeO_2 catalysts calcined at different temperatures were collected on a Rigaku X-ray diffractometer (DMAX IIIVC) in the range of $2\theta = 20°\text{-}70°$. TEM micrographs of synthesized catalysts were produced on Tecnai G^2-20 Twin (FEI) transmission electron microscope operated at 200 kV. Raman spectra were obtained on a Horiba JY Lab RAM HR 800 Raman spectrometer with a 514 nm excitation laser source and a spectral resolution of 0.3 cm^{-1}. The amount of Pd in Pd-CeO_2 catalysts was confirmed using ARCOS, Simultaneous ICP-AES spectrometer.

2.3. Catalytic experiments

The heterogeneous catalytic gas-phase hydrogen-iodide decomposition experiments were performed in a quartz reactor (tube of 16 mm diameter) under atmospheric pressure as shown in figure 1. 1 g of prepared nanocatalyst was used in each experiment conducted at different constant temperatures ranging from 400°C-550°C. The 55 wt % aqueous hydrogen-iodide was allowed to flow at a weight-hourly-space velocity

(WHSV) of 12.9 h^{-1}. The carrier gas (nitrogen) was passed through the reactor at constant flow rate of 40 ml/min. Hydrogen-iodide, iodine, and water were trapped in sodium thiosulphate and sodium hydroxide scrubbers and a condenser, respectively, allowing only hydrogen generated and nitrogen to flow into a gas chromatograph. A gas chromatograph (Nucon-5765) was used to analyze the hydrogen produced in the process.

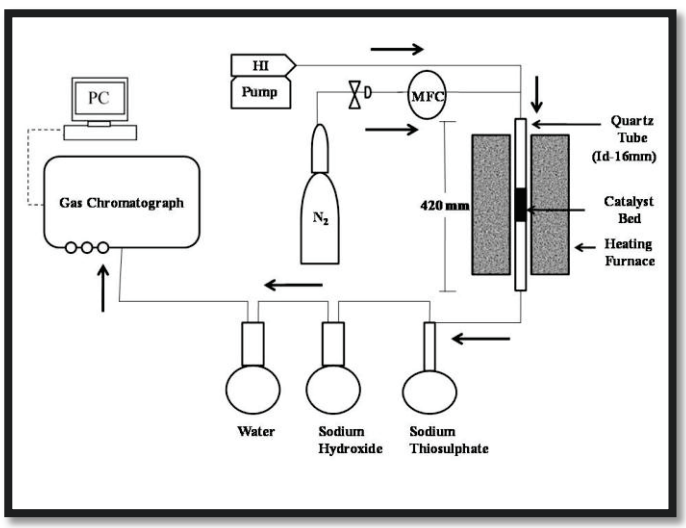

Figure 1. Schematic diagram of the experimental set-up for hydrogen-iodide decomposition using Pd-CeO_2 catalysts.

3. Results and discussion

3.1. Catalyst characterization

Table 1. Sample characterization.

Sample[a]	Theoretical Pd (%)	Actual Pd[a] (%)	Specific surface area[b] (m^2 g^{-1})	Crystallite size[c] (nm)	Lattice constants (Å)
Pd-CeO_2–300	2.0	2.0	91.2	6.1	5.412
Pd-CeO_2–500	2.0	2.0	54.5	14.6	5.411
Pd-CeO_2–700	2.0	2.0	18.9	45.1	5.410

[a]confirmed by ICP-AES. [b]BET surface area. [c]calculated using Debye-Scherrer equation applied to (111) plane.

The specific surface areas of the prepared Pd-CeO_2 catalysts were measured by BET technique, based on nitrogen adsorption (table 1). The specific surface area is 91.2 $m^2 g^{-1}$ for Pd-CeO_2–300, 54.5 $m^2 g^{-1}$ for Pd-CeO_2–500, and 18.9 $m^2 g^{-1}$ for Pd-CeO_2–700, respectively; thus with an increase in the calcination temperature the specific surface area of the Pd-CeO_2 catalyst decreases.

The powder XRD patterns of the prepared Pd-CeO_2 catalysts calcined at different temperatures are shown in figure 2. All the diffraction patterns showed sharp peaks of cubic fluorite structure of CeO_2 at 28.6°, 33.1°, 47.5°, 56.4°, and 59.1° corresponding to (111), (200), (220), (311), and (222) planes, respectively [22]. No peaks of Pd are however observed in the diffraction patterns of any of the catalyst samples indicating the formation Pd-Ce solid solutions. The average crystallite sizes of the prepared Pd-CeO_2 materials were calculated from X-ray data using Debye-Scherrer equation:

Average crystallite size, $D = 0.9\lambda/\beta cos\theta$ (4)

,where β is the full-width at half-maximum (FWHM) measured in radians, λ the X-ray wavelength of Cu-Kα radiation, and θ, the Bragg's angle.

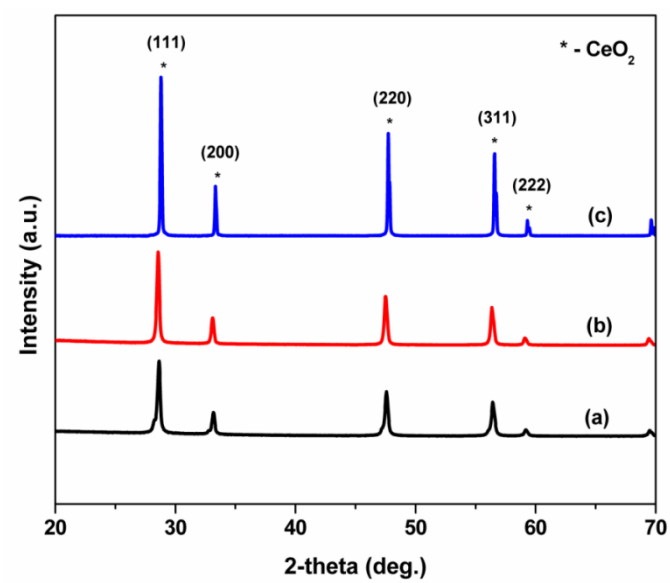

Figure 2. Powder XRD patterns of (a) Pd-CeO_2-300; (b) Pd-CeO_2-500; and (c) Pd-CeO_2-700.

The lattice parameters were calculated to be around 5.412 Å, 5.411 Å, and 5.410 Å for Pd-CeO_2-300, Pd-CeO_2-500, and Pd-CeO_2-700 with the help of Bragg's law. The ionic radii of Pd^{2+} and Ce^{4+} are 0.86 Å and 0.97 Å. This indicates that Pd^{2+} ions have dissolved into ceria lattice instead of Ce^{4+} ions through sol-gel method. The calculated average crystallite sizes of Pd-CeO_2-300, Pd-CeO_2-500, and Pd-CeO_2-700 were found to be 6.1, 14.6, and 45.1 nm, respectively, with the help of Debye-Scherrer equation applied to (111) plane (table 1). With an increase in the calcination temperature, the peak intensity and sharpness increases which indicate a decrease in FWHM values, i.e. increase in crystallite sizes. This is in a good agreement with the BET surface area values which also showed a decrease in the surface area with an increase in the calcination temperature.

The TEM micrographs of Pd-CeO_2-300, Pd-CeO_2-500, and Pd-CeO_2-700 catalyst samples are shown in figures 3(a) to 3(c). TEM analyses of all the catalysts revealed the spherical nanosized particles. It is observed that the particle size of the catalyst also increased with an increase in the calcination temperature. The average particle size of Pd-CeO_2-300, Pd-CeO_2-500, and Pd-CeO_2-700 are 8.3, 15.2, and 48.6 nm. These results are again in agreement with the powder XRD and BET results.

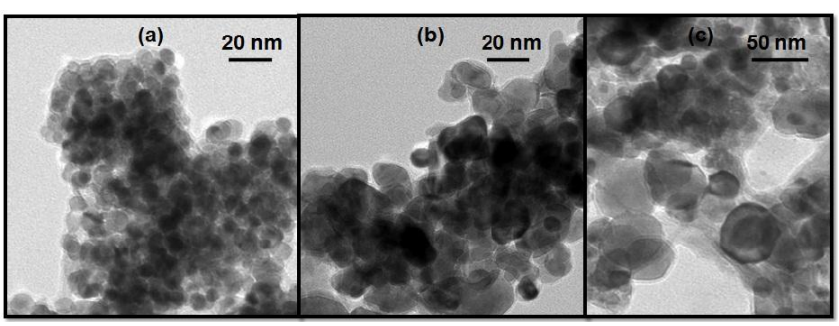

Figure 3. TEM micrographs of (a) Pd-CeO_2-300; (b) Pd-CeO_2-500; and (c) Pd-CeO_2-700.

Raman spectroscopy is an important characterization technique to confirm the phases and defects present in the materials. Figure 4 represents Raman spectra (200-1600 cm^{-1}) of Pd-CeO_2 catalyst materials calcined at different temperatures. Raman spectra of all the materials exhibit a cubic fluorite structure with an

F_{2g} Raman active vibrational mode at 464.5 cm^{-1} [34]. A small Raman band at around 588 cm^{-1} corresponds to the defect mode, D bond (oxygen vacancy). The intensity ratio, I_D/I_{F2g} gives the degree of defects present in Pd-CeO_2 [35]. The intensity ratio follows the order: Pd-CeO_2-300 > Pd-CeO_2-500 > Pd-CeO_2-700. This implies that Pd-CeO_2-300 possessed a larger number of oxygen vacancies when compared to Pd-CeO_2-500, and Pd-CeO_2-700. The smaller intensity and larger broadening (larger FWHM in the Raman spectra) of Pd-CeO_2-300 sample indicate smaller nanosized particles in it as compared to those in Pd-CeO_2-500 and Pd-CeO_2-700 catalysts. Thus, the results of Raman spectra are consistent with those of XRD and TEM results.

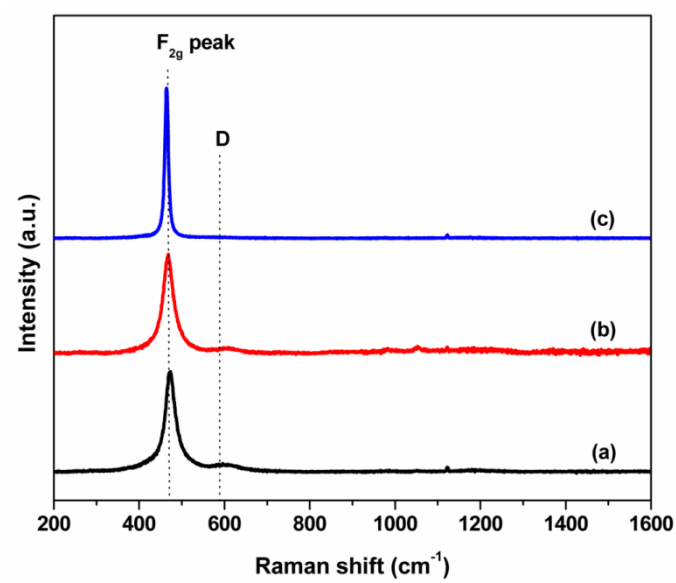

Figure 4. Raman spectra of (a) Pd-CeO_2-300; (b) Pd-CeO_2-500; and (c) Pd-CeO_2-700.

3.2. Catalytic activity

The results of hydrogen-iodide decomposition experiments at different temperatures over synthesized Pd-CeO_2 nanocatalysts are shown in figure 5. The hydrogen-iodide conversion on Pd-CeO_2-700 is about 12.3 % at 400°C. With the increase in temperature, the hydrogen-iodide conversion on Pd-CeO_2-700 increased. It showed a conversion of 19.1 % at 550°C. Pd-CeO_2-300 and Pd-CeO_2-500, on the other hand gave very high conversions at 550°C, reaching about 23.3 % (close to the theoretical equilibrium value of 24 % at 550°C)

and 21.7 %, respectively. At 400°C, the latter two catalysts showed conversions of around 17.7 % and 15.5 %, respectively. It is thus observed that the hydrogen-iodide conversion decreased with the increase in the catalyst-calcination temperature. Pd-CeO_2-300 HI conversion of 23.3% showed greater catalytic activity than the other catalysts at 550°C (Pt-CeO_2 (22.0%) [26], Ni-CeO_2 (21.0%) [36], and CeO_2 (19.4%) [22]).

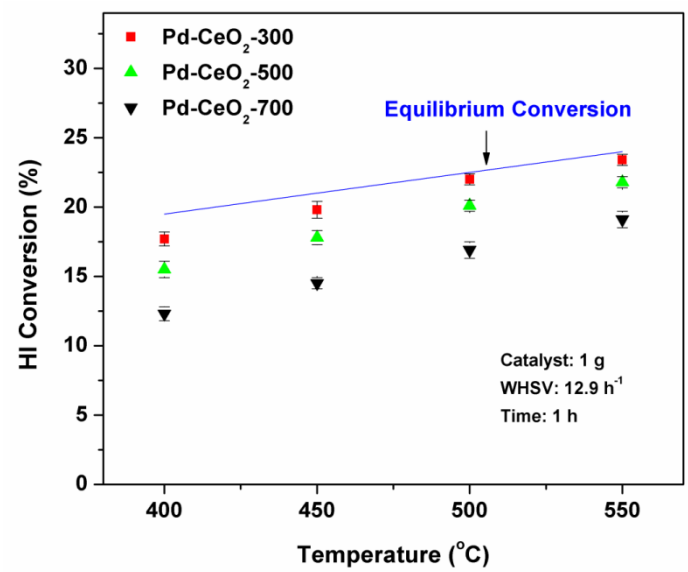

Figure 5. Hydrogen-iodide conversion over Pd-CeO_2 catalysts at different decomposition temperatures (HI-55 wt %).

These catalytic performance results are supported well by those from characterizations using BET, XRD, TEM, and Raman spectroscopy. With an increase in the calcination temperature, the average particle size increased and the specific surface area and oxygen vacancies decreased, and thus the catalytic activity for hydrogen-iodide decomposition reaction decreased. The oxygen vacancy plays the dominant role in surface reactions of hydrogen-iodide decomposition [16]. According to Zhang *et al.* [16] new reaction mechanism for hydrogen-iodide decomposition over CeO_2 catalyst, HI is adsorbed first and activated on the surface of Pd-CeO_2 through the oxygen vacancy causing the cleavage of H–I.

The time-on-stream stability test is also conducted for Pd-CeO_2-300 catalyst for 5 h. Figure 6 shows the time-on-stream stability test data for Pd-CeO_2-300 catalyst. For this purpose, 1 g of catalyst, at a

temperature of 500°C, and WHSV of 12.9 h^{-1}, was used. A nearly constant hydrogen-iodide conversion of 22.0 % was observed during the whole time-on-stream of 5 h at 500°C. No deactivation of the catalyst was observable at all, which indicates its good stability at the operating temperature of interest in practice.

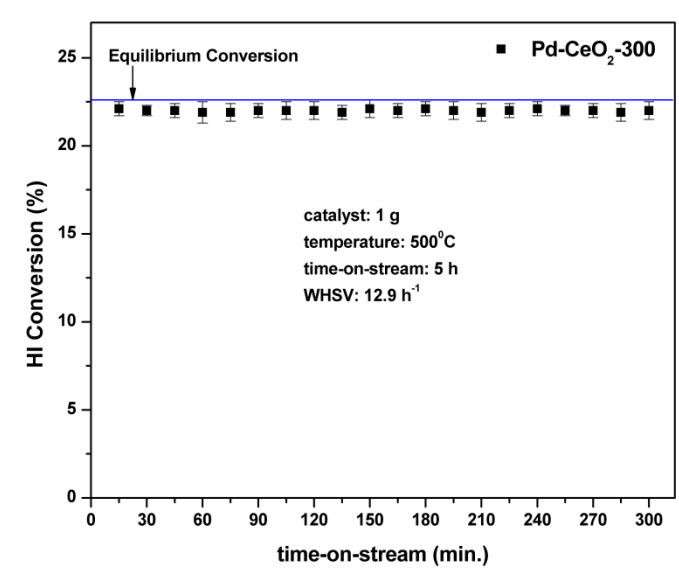

Figure 6. Time-on-stream stability test of Pd-CeO_2-300 catalyst for hydrogen-iodide conversion (Operating conditions: Catalyst-1 g, temperature-500°C, WHSV-12.9 h^{-1}, time-on-stream-5 h, HI-55 wt %).

4. Conclusions

Pd-CeO_2 catalysts were successfully synthesized by sol-gel method and by employing different calcination temperatures. BET, XRD, TEM, and Raman studies revealed that an increase in the calcination temperature resulted into smaller specific surface areas, larger average particle sizes, and smaller numbers of oxygen vacancies. Pd-CeO_2-300 possessing a high specific surface area, smaller average particle size, and larger number of oxygen vacancies, achieved near-equilibrium conversions at 550°C and a WHSV of 12.9 h^{-1}. Also, this Pd-CeO_2-300 nanocatalyst showed reasonable stability for the time-on-stream of 5 h at 500°C without any observable deactivation.

Further work is in progress to test the activity of Pd-CeO_2 catalyst for much longer times-on-stream

of 50 h – 100 h.

Acknowledgements

This work was supported by the ONGC Energy Centre Trust (OECT) [RP02148], India.

References

[1] Singhania A, Bhaskarwar AN, Damaraju P, Bhardwaj A, Prabhu BN, Thomas NJ, Kale DM. Highly active supported bimetallic (Ni-Pt) catalyst for hydrogen iodide (HI) decomposition and synthesis procedure thereof. IN Patent 2259/DEL/2014 2014.

[2] Oosawa Y, Kumagai T, Mizuta S, Kondo W, Takemori Y, Fujii K. Kinetics of the catalytic decomposition of hydrogen iodide in the magnesium–iodine thermochemical cycle. Bull Chem Soc Jpn 1981;54:742–8.

[3] Goldstein S, Borgard JM, Vitart X. Upper bound and best estimate of the efficiency of the iodine sulphur-cycle. Int J Hydrogen Energy 2005;30(6):619-26.

[4] Singhania A, Krishnan VV, Bhaskarwar AN, Bhargava B, Parvatalu D, Banerjee S. Hydrogen production from the decomposition of hydrogen iodide over nanosized NiO-ZrO_2 catalysts prepared by solution combustion techniques. Catal Comm 2017;93:5-9.

[5] Kim JM, Park JE, Kim YH, Kang KS, Kim CH, Park CS, Bae KK. Decomposition of hydrogen iodide on Pt/C-based catalysts for hydrogen production. Int J Hydrogen Energy 2008;33(19):4974-80.

[6] O'Keefe DR, Norman JH, Williamson DG. Catalysis research in thermochemical water-splitting processes. Catal Rev 1980;22(3):325-69.

[7] Favuzza P, Felici C, Lanchi M, Liberatore R, Mazzocchia CV, Spadoni A, Tarquini P, Tito AC. Decomposition of hydrogen iodide in the S-I thermochemical cycle over Ni catalyst systems. Int J Hydrogen Energy 2009;34(9):4049-56.

[8] Singhania A, Krishnan VV, Bhaskarwar AN, Bhargava B, Parvatalu D, Banerjee S. Catalytic performance of bimetallic Ni-Pt catalyst supported on activated carbon, gamma- alumina, zirconia and ceria for hydrogen production in sulphur-iodine thermochemical cycle. Int J Hydrogen Energy 2016;41(25):10538-46.

[9] Li D, Wang L, Zhang P, Chen S, Xu J. Effects of the composition on the active carbon supported Pd-Pt bimetallic catalysts for HI decomposition in the iodine-sulfur cycle. Int J Hydrogen Energy 2013;38(16):6586-92.

[10] Wang L, Hu S, Li D, Han Q, Zhang P, Chen S, Xu J. Effects of the second metals on the active carbon supported Pt catalysts for HI decomposition in the iodine-sulfur cycle. Int J Hydrogen Energy 2014;39(26):14161-65.

[11] Wang Z, Wang L, Chen S, Zhang P, Xu J, Chen J. Decomposition of hydrogen iodide over Pt-Ir/C bimetallic catalyst. Int J Hydrogen Energy 2010;35(17):8862-67.

[12] Singhania A, Bhaskarwar AN, Damaraju P, Bhardwaj A, Prabhu BN, Thomas NJ, Kale DM. Vanadia supported Pt catalyst and use thereof for hydrogen iodide decomposition in sulphur-iodine (SI) cycle for hydrogen production. IN Patent 2308/DEL/2014 2014.

[13] Zhang Y, Wang Z, Zhou J, Liu J, Cen K. Catalytic decomposition of hydrogen iodide over pre-treated Ni/CeO_2 catalysts for hydrogen production in the sulfur-iodine cycle. Int J Hydrogen Energy 2009;34(21):8792-8.

[14] Favuzza P, Felici C, Nardi L, Tarquini P, Tito A. Kinetics of hydrogen iodide decomposition over activated carbon catalysts in pellets. Appl. Catal. B Environ. 2011;105(1-2):30-40.

[15] Wang L, Zhang P, Chen S, Xu J. Overview of the development of catalysts for HI decomposition in the iodine-sulfur thermochemical cycle at INET. Nucl. Eng. Des. 2014;271:60-63.

[16] Chen Y, Wang Z, Zhang Y, Zhou Z, Cen K. Platinum-ceria-zirconia catalysts for hydrogen production in sulfur-iodine cycle. Int J Hydrogen Energy 2010;35(2):445-51.

[17] Wang ZC, Wang LJ, Zhang P, Chen SZ, Xu JM, Chen J. Effect of preparation methods on Pt/alumina catalysts for the hydrogen iodide catalytic decomposition. Chin Chem Lett 2009;20(1):102-5.

[18] Tyagi D, Varma S, Bharadwaj SR. Pt/Zirconia catalyst for hydrogen generation from HI decomposition reaction of S–I cycle. Int J Energy Res 2015;39(4):484-93.

[19] Wang L, Bai S, Wang Z, Zhao Y, Yuan X, Zhang P, Chen S, Xu J, Meng X. Activity and stability of Pt catalysts supported on carbon nanotubes, active carbon and γ-Al_2O_3 for HI decomposition in iodine-sulfur thermochemical cycle. Int J Hydrogen Energy 2012;37(13):10020-7.

[20] Wang L, Han Q, Li D, Wang Z, Chen J, Chen S, Zhang P, Liu B, Wen M, Xu J. Comparisons of Pt catalysts supported on active carbon, carbon molecular sieve, carbon nanotubes and graphite for HI decomposition at different temperatures. Int J Hydrogen Energy 2013;38(1):109-16.

[21] Wang L, Li D, Zhang P, Chen S, Xu J. The HI catalytic decomposition for the lab-scale H_2 producing apparatus of the iodine-sulfur thermochemical cycle. Int J Hydrogen Energy 2012;37(8):6415-21.

[22] Zhang Y, Wang Z, Zhou J, Cen K. Ceria as a catalyst for hydrogen iodide decomposition in sulfur–iodine cycle for hydrogen production. Int J Hydrogen Energy 2009;34(4):1688-95.

[23] Yao HC, Yao YFY. Ceria in automotive exhaust catalysts I. Oxygen storage J Catal 1984;86(2):254-65.

[24] Stefanik TS, Tuller HL. Ceria-based gas sensors. J Eur Ceram Soc 2001;21(10-11):1967-70.

[25] Caputo F, De Nicola M, Sienkiewicz A, Giovanetti A, Bejarano I, Licoccia S, Traversa E, Ghibelli L. Cerium oxide nanoparticles, combining antioxidant and UV shielding properties, prevent UV-induced cell damage and mutagenesis.

Nanoscale 2015;7(38):15643-56.

[26] Zhang Y, Wang Z, Zhou J, Liu J, Cen K. Effect of preparation method on platinum-ceria catalysts for hydrogen iodide decomposition in sulfur-iodine cycle. Int J Hydrogen Energy 2008;33(2):602-7.

[27] Fan J, Wu XD, Ran R, Weng D. Influence of the oxidative/reductive treatments on the activity of $Pt/Ce_{0.67}Zr_{0.33}O_2$ catalyst. Appl Surf Sci 2005;245(1-4):162-71.

[28] www.icmj.com/current-metal-prices.php dated: 21.04.2017.

[29] LuO MF, Song YP, Lu JQ, Wang XY, Pu ZY. Identification of CuO species in high surface area $CuO-CeO_2$ catalysts and their catalytic activities for CO oxidation. J Phys Chem C 2007;111(34):12686-92.

[30] Teng F, Xu P, Tian Z, Xiong G, Xu Y, Xu Z, Lin L. Synthesis of the high- surface-area $Ce_xBa_{1-x}MnAl_{11}O_y$ catalyst in reverse microemulsions using inexpensive inorganic salts as precursors. Green Chem 2005;7(7):493-9.

[31] Wang H, Zhu JJ, Zhu JM, Liao XH, Xu S, Ding T, Chen HY. Preparation of nanocrystalline ceria particles by sonochemical and microwave assisted heating methods. Phys Chem Chem Phys 2002;4(15):3794-99.

[32] Hirano M, Inagaki M. Preparation of monodispersed cerium (IV) oxide particles by thermal hydrolysis: Influence of the presence of urea and Gd doping on their morphology and growth. J Mater Chem 2000;10(2):473-7.

[33] Singhania A, Gupta SM. Nanocrystalline ZrO_2 and Pt-doped ZrO_2 catalysts for low-temperature CO oxidation. Beilstein J Nanotechnol 2017;8:264-71.

[34] Santos MLD, Lima RC, Riccardi CS, Tranquilin RL, Bueno PR, Varela JA, Longo E. Preparation and characterization of ceria nanospheres by microwave-hydrothermal method. Mater Lett 2008;62(30):4509-11.

[35] Lin J, Li L, Huang Y, Zhang W, Wang X, Wang A, Zhang T. In situ calorimetric study: Structural effects on adsorption and catalytic performances for CO oxidation over Ir-in- CeO_2 and Ir-on-CeO_2 catalysts. J Phys Chem C 2011;115(33):16509-17.

[36] Zhang Y, Zhou J, Chen Y, Wang Z, Liu J, Cen K. Hydrogen iodide decomposition over nickel-ceria catalysts for hydrogen production in the sulphur-iodine cycle. Int J Hydrogen Energy 2008;33(20):5477-83.